

# Simulating (100) diamond chemical vapour deposition using a 3D kinetic Monte Carlo code with a tetrahedral model for diamond

Max D. G. Williams, Paul W. May & Neil L. Allan

**To cite this article:** Max D. G. Williams, Paul W. May & Neil L. Allan (2025) Simulating (100) diamond chemical vapour deposition using a 3D kinetic Monte Carlo code with a tetrahedral model for diamond, *Functional Diamond*, 5:1, 2557914, DOI: [10.1080/26941112.2025.2557914](https://doi.org/10.1080/26941112.2025.2557914)

**To link to this article:** <https://doi.org/10.1080/26941112.2025.2557914>



© 2025 The Author(s). Published by Informa UK Limited, trading as Taylor & Francis Group, on behalf of Zhengzhou Research Institute for Abrasives & Grinding Co., Ltd.



[View supplementary material](#)



Published online: 13 Sep 2025.



[Submit your article to this journal](#)



Article views: 147



[View related articles](#)



[View Crossmark data](#)

RESEARCH ARTICLE



# Simulating (100) diamond chemical vapour deposition using a 3D kinetic Monte Carlo code with a tetrahedral model for diamond

Max D. G. Williams, Paul W. May , and Neil L. Allan 

School of Chemistry, University of Bristol, Cantock's Close, Bristol, United Kingdom

## ABSTRACT

An on-lattice, *N*-fold, variable-time-step, periodic kinetic Monte Carlo model for {100} chemical vapour deposition (CVD) diamond growth has been developed using a 3-dimensional fully tetrahedral model for the diamond lattice. The growth model supports adsorption and incorporation of  $\text{CH}_x$  species at monoradical and biradical dimer and trough sites. Once  $\text{CH}_x$  has been incorporated into the lattice as a  $\text{CH}_2$  bridge, they can be rapidly etched back into the gas phase using a preferential-etching mechanism, or migrate across the surface until they eventually fuse and add to the bulk. The new 3D model has enabled three migration events to be specified and modelled in more detail: adjacent dimer migration, migration into vacant trough sites and migration down atomic steps. Specific dimer-creation and dimer-breaking processes have also now been added to the 3D model, and these dimer reconstructions on the surface are now modelled explicitly. Inclusion of both mechanisms simultaneously increased predicted growth rates and decreased roughness for nanocrystalline and microcrystalline diamond growth conditions. The conclusion is that future kMC models need to include the three migration events as well as models for dimer making and breaking processes if they are to simulate diamond growth more accurately.

## ARTICLE HISTORY

Received 23 May 2025

Accepted 3 September 2025

## KEYWORDS

CVD diamond; kinetic Monte Carlo; modelling of growth; surface migration

## 1. Introduction


Chemical vapour deposition (CVD) of diamond [1] is now a mature technology with many existing and potential commercial applications in electronics, quantum computing, mechanical parts, sensors, optics and jewellery [2]. Advances in CVD technology driven by the burgeoning market in lab-grown diamond gemstones [3], have allowed thicker diamond films to be deposited at faster rates, and therefore at lower cost. The previous commonly held perception that diamond is a rare and expensive product only useful for gems or niche applications is being dispelled rapidly, and finally diamond is becoming regarded as a truly useful, affordable, engineering material [4].

In CVD, a diamond coating is deposited onto the surface of a suitable substrate, which may be a smaller diamond seed in the case of gemstone growth, or materials such as a Si wafer, a quartz window, or metal surface for mechanical-wear applications. The substrate is placed onto a heated stage (700–1000 °C) inside a vacuum chamber containing flowing process gases at 20–200 torr. The gases typically comprise a carbon source, such as methane, diluted to just a few percent input mole fraction in hydrogen. These gases are energised using either a heated metal (W, Ta, or Re) filament

placed a few mm above the substrate surface or by application of a microwave discharge. The thermal or electrical energy fragments the molecules to form a chemical “soup” of atoms, radicals, ions and clusters near the substrate surface. Reactive species, mainly H atoms and  $\text{CH}_3$  radicals, from this hot gas mixture diffuse to the surface, and under certain optimal conditions [5], deposit onto the surface as a continuous layer of diamond.

Different applications require diamond films with different properties and compositions. Whatever the application, optimisation of the diamond CVD process is crucial to achieve the desired diamond characteristics. Most experimental and theoretical studies of diamond growth have focused on the (100) diamond surface, because growth here leads to fewer defects than on other surfaces and can produce large, flat terraces of near perfect crystallinity under optimal conditions. Although a “standard model” for diamond growth [6] has existed for over 20 years, it fails to account fully for the growth rate, the crystallite size, defect incorporation, and many other growth features observed experimentally. In the standard model, H atoms are created by the dissociation of  $\text{H}_2$  in the plasma or thermally by the filament. These drive the chemical processes both in the gas phase and on the diamond surface, creating surface-radical sites

**CONTACT** Paul W. May  [paul.may@bristol.ac.uk](mailto:paul.may@bristol.ac.uk)

 Supplemental data for this article can be accessed online at <https://doi.org/10.1080/26941112.2025.2557914>.

© 2025 The Author(s). Published by Informa UK Limited, trading as Taylor & Francis Group, on behalf of Zhengzhou Research Institute for Abrasives & Grinding Co., Ltd.

This is an Open Access article distributed under the terms of the Creative Commons Attribution License (<http://creativecommons.org/licenses/by/4.0/>), which permits unrestricted use, distribution, and reproduction in any medium, provided the original work is properly cited. The terms on which this article has been published allow the posting of the Accepted Manuscript in a repository by the author(s) or with their consent.

(dangling bonds) by abstraction of H from the C–H surface bonds. The fraction of surface radical sites is ~10% [7], depending upon the process conditions, such as the concentration of gas-phase atomic H just above the surface,  $[H]_g$ , and the substrate temperature,  $T_s$ . The main growth species is believed to be the  $CH_3$  radical [8–10], which adds to these surface-radical sites. Because the substrate temperature is high ( $T_s > 700^\circ\text{C}$ ), these chemisorbed species may migrate across the surface until they meet a step-edge, where they permanently attach themselves to the diamond lattice and lead to step-flow growth [11], or be etched back into the gas phase via a further reaction with gas-phase atomic H.

Although much of the diamond-growth development work has been performed experimentally by trial-and-error, a deeper understanding of the multiple interconnected processes underlying the CVD process has also been achieved using computer simulation [12]. Such simulations can be powerful predictive tools to understand the effect of molecular interactions on the final film morphology and growth rate. Detailed *ab initio* quantum-mechanical calculations are useful to study specific chemical-reaction mechanisms, such as  $CH_3$  addition to the surface and migration [8], but arguably the most successful approach has been kinetic Monte Carlo (kMC) simulation [13], which can model the deposition of dozens of layers of diamond in reasonable computational time. Such kMC simulations are based on a model diamond (100) surface and use a chosen set of relevant processes, such as adsorption, etching/desorption, migration, with known (or estimated) rates and energies. At each step of the simulation, a process is chosen with a probability proportional to its rate. Over the past 20 years, these kMC simulations have become more sophisticated as the gas-phase and gas-surface interactions have become better understood [14–21]. Indeed, commercial software is now available that models these gas-phase reactions and species concentrations within a user-specified reactor geometry [22]. A review of many previous kMC simulations of diamond growth by ourselves and other groups is given in Ref. [21], so for brevity, here, we shall briefly only discuss three models from other groups, that have been the most successful in reproducing experimental observations of diamond growth, as well as our own previous kMC model to put the current work into context.

In 1999–2000, Griotic & Lai developed a diamond growth simulation which combined reactor-scale and atomic-scale models [18–20]. They used a model for diamond (111) and (100) surfaces with a database of 12 gas-surface reactions together with the one-dimension computer codes CHEMKIN/SPIN to produce a kMC simulation which, despite its relative simplicity, predicted the temperature dependence of growth rate and film quality which were reasonably consistent with experiment. However, the simulation did not include surface migration, which is believed to be crucial in

determining film growth and morphology. Also, their 1D gas model was unable to simulate accurately the transport and reactions occurring in a 3D CVD chamber, and as a result, the gas concentrations at the diamond surface (particularly those for atomic H) were overestimated by perhaps a factor of ~10–100, meaning fitting parameters were required to scale the growth rates to match experimental values.

Results from another sophisticated kMC simulation were reported by Netto and Frenklach [23] who used methyl radicals as the sole growth species incorporated into the diamond surface by means of a ring-opening/closing mechanism.  $CH_2$  migration mechanisms along and across the dimer rows were included, as well as the reforming of dimer-reconstructed bonds from two suitable adjacent surface radical sites. Etching was only considered to occur at isolated incorporated  $CH_2$  groups and reconstructed dimers. Overall, their simulations showed that  $CH_3$  can adsorb at random positions upon a diamond surface and then migrate until multiple species coalesce. However, their model could not simulate the variation in surface morphology with deposition conditions.

The most recent reported kMC simulation is by Valentin et al. [24] who extended the models from a number of previous simulations [6,17,21,23] using a cubic 3D representation of the (100) diamond lattice. The model considers adsorption and desorption of  $CH_3$  radicals, etching of carbon atoms, and migration of adsorbed radicals, using the adsorption/insertion, migration and etching reactions and the rates from previous reports. Their model, however, now assumes that etching is much less aggressive, and adopts the premise that insertions only happen at dimers. The model also assumes that desorption only occurs to non-inserted species – which prevents dimers from forming away from step-edges. These assumptions essentially force step-flow growth such that the diamond lattice is enlarged only by extension of the dimer rows. Unsurprisingly, this model reproduces the step-flow growth mechanism seen on diamond (100) surfaces, along with step bunching when non-etchable “defects” are introduced to a dimer row. While it is encouraging for growth models to replicate behaviour previously seen in experiment, the energetics and therefore the plausibility of the above assumptions should be investigated using modern *ab initio* methods before a contribution to theoretical understanding can be attributed.

Our group have previously reported the development of a 3D kMC model to simulate diamond (100) CVD under conditions used to grow single-crystal diamond (SCD), microcrystalline diamond (MCD), nanocrystalline diamond (NCD), and ultrananocrystalline diamond (UNCD) films [21]. The model included adsorption of  $CH_x$  ( $x=0, 3$ ) species, insertion of  $CH_y$  ( $y=0-2$ ) into surface dimer bonds, etching/desorption of both

transient adsorbed species and lattice sidewalls, lattice incorporation, and surface migration, but not defect formation or renucleation processes. SCD and MCD growths were found to be dominated by migration and step-edge growth, whereas in NCD and UNCD growth, migration occurred less frequently, and species tended to nucleate where they landed. Etching of species from the lattice sidewalls was modelled as a function of the number of bonded neighbours, allowing flat-bottomed and/or sharp-pointed etch pits to be simulated, consistent with those seen in experiment. Other observed growth phenomena, such as needles and hillocks, were also simulated using unetchable, immobile species as surface defects.

Despite the qualitative and quantitative successes of this model (albeit with fitting parameters), because it represented diamond as a cubic, rather than a tetrahedral structure, detailed insight into specific defect formation and growth mechanisms was not possible. Therefore, the entire code has now been reconfigured using a more realistic model for the diamond lattice which can be visualized as two interpenetrating face-centred cubic lattices, offset along the body diagonal by one-quarter of its length, such that each bulk carbon atom is tetrahedrally bonded to four neighbouring atoms. The “dangling bonds” at the surface are terminated with hydrogen. Predictions of growth rates and film roughness as a function of growth condition, such as  $\text{CH}_3$  concentration, substrate temperature, migration, and many other growth parameters are largely in agreement with the previous cubic model, and with experimental results obtained under a range of different diamond CVD conditions, from single-crystal growth to UNCD. Therefore, there is no need to restate these results here. The full details of the implementation of this new kMC code along with these results can be found in Ref. [25].

In this paper, we instead focus on some new aspects of the simulation that have been added to the kMC growth model to determine their importance in the diamond growth process. In particular, these include a description for the making and breaking of surface dimers, and what role these processes play in adsorption of gas-phase species, surface migration, and etching.

## 2. Simulation details

### 2.1. Representing the (100):H diamond surface

Only a brief discussion of the kMC model will be given here, as the full details can be found in Ref. [25]. The diamond surface is represented by a square supercell perpendicular to the [100] direction. The growth surface is initialised to be atomically smooth, fully  $2 \times 1$  reconstructed [26] and with each surface carbon implicitly terminated by a single hydrogen atom, rendering it chemically passivated. During the simulation, the diamond lattice is fixed at a substrate temperature ( $T_s$ ), which is usually known via experimental pyrometry measurements, and interacts with an infinite bath of hot gas-species near to the surface at the “near-surface” temperature ( $T_{ns}$ ) via gas-surface reactions. In practice, the assumption that  $T_{ns} \sim T_s$  is found to have no significant effect upon calculated growth rates or surface roughness. An example of the initial arrangement of the surface carbons is shown in Figure 1.

Given the high Debye temperature of diamond ( $\sim 1900$  K [27]), little to no spontaneous bulk rearrangement or significant vibrational effects are expected at CVD temperatures (900–1200 K), and can be safely neglected [27,28]. Dimer reconstruction of the surface is modelled explicitly and carbons are visually displaced from their bulk lattice positions. Dimer formation and breaking are key processes in the growth model which were difficult to model properly using previous cubic models of the diamond lattice. Being able to simulate these processes accurately in a 3D tetrahedral model has important implications for the growth mechanism, as discussed in Section 4.

Positions filled by a carbon atom which does *not* have 4 C–C bonds are considered to be a “surface atom” ( $C_s$ ) and therefore chemically active, while bulk carbon atoms which have formed 4 C–C bonds, are not part of the surface and chemically inactive. Empty positions adjacent to surface atoms are considered to be active during rate setting, as they represent positions which could be filled in the upcoming kMC iteration. Therefore, unfilled positions at the surface are called *surface sites* while filled positions with bulk and sub-bulk bonding are called *atoms* and *surface atoms*, respectively. Finally, the model employs periodic boundary conditions along the lateral directions ( $x, y$ ) to prevent the possibility of crystal-edge effects.

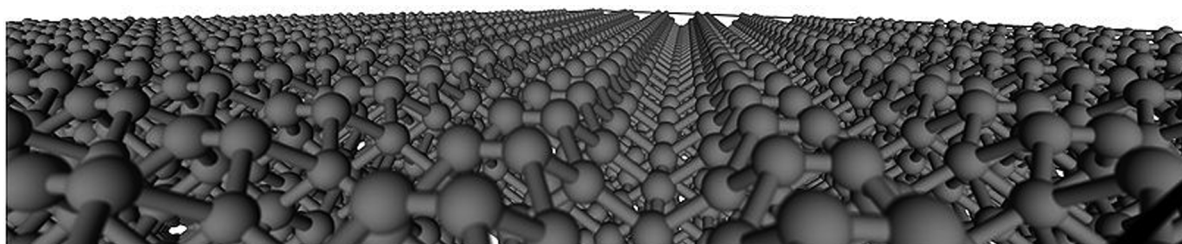


**Figure 1.** The  $2 \times 1$  reconstructed, mono-hydrogenated initial (100) diamond simulation surface, showing the long parallel dimer rows. Note that hydrogens are not displayed here.



## 2.2. Specifying the growth conditions

Gas-species concentrations are taken from modelling of microwave (MW) and hot filament (HF) reactors by May and Mankelevich [29,30]. These models capture both the interactions between the reactive gas mixture and the activation source as well as chemical reactions between the reactive species, along with their interactions with the reactor walls and the growth surface. The known experimental conditions – power, pressure, gas mixture and flow, and substrate temperature – for these reactors growing SCD, MCD, NCD and UNCD films – were used as inputs in the gas-phase model of the reactors, resulting in a set of concentrations for the stable and reactive gas-phase species situated ~0.5 mm above the growing diamond surface. More information on these reactor models can be found in Refs. [30–33].

A complication is that as gas molecules approach closer than a few 100  $\mu\text{m}$  to the growing diamond surface they enter a “boundary layer” where there can be huge gradients of temperature, gas flow and species concentration, thus making the true flux of species to the growth surface itself rather uncertain [34]. The species concentrations at the growth surface were therefore approximated by treating the gaseous region close to the surface ( $z < 0.5$  mm) as a “compressed version” of the gas above the filament or plasma ball, neglecting any surface-diffusion effects, and taking the gas concentration at the surface to be the species concentration above the filament/plasma ball where the temperature is the same as the surface [17]. We assume that any carbon growth species can only significantly contribute to the growth process if it has near-surface concentrations above  $1 \times 10^9 \text{ cm}^{-3}$  [17]. Below this threshold, the calculated rates of flux with the surface are too low for species to incorporate at meaningful rates. The extrapolated values of gas-phase species concentrations are given in Table S1 in the Supplementary Information (and also in Ref. [17]).

## 2.3. Growth simulation

The simulations follow a standard kMC algorithm. Following initialisation of the supercell (Section 2.1), reaction rates are calculated from the growth conditions (Section 2.2) defined in the input. A growth simulation occurs via repeated execution of events (reactions, migrations, *etc.*) chosen at random from a set of possible events. After the execution of an event, the simulation time is incremented utilising a variable time-step

$$\Delta t = -\frac{\ln r}{\sum_i^N v_i} \quad (1)$$

where  $r$  is a random number between 0 and 1,  $N$  is the number of potential event pathways,  $i$ , each having a rate  $v_i$ , and  $\sum_i^N v_i$  is the sum of all possible rates in the system. A single kMC iteration involves the following steps:

1. Each surface atom is considered for activation or deactivation according to the predicted monoradical-site fraction,  $F_{\text{mr}}$  (Section 2.4).
2. The possible reactions of each surface atom and site are used to construct a rate list of available reaction events and their rates (Section 2.5), and also a weighted rate array (WRA) by multiplying each event by its rate (Section 2.5).
3. A pseudo-random choice is made from the WRA to decide which event to execute from the rate list.
4. The chosen event is executed, and the system state evolved accordingly (Section 2.6).
5. The calculated simulation time is incremented by  $\Delta t$  given by Equation (1).

## 2.4. Surface activation

Interactions of gaseous H and  $\text{H}_2$  with the surface (such as abstractions and additions) are not modelled explicitly. This implicit approach to monoradical-site creation, sometimes described as a “super-basin approximation” [21], is often used in kMC calculations and is valid provided the rates of all the other processes are not too dissimilar. Due to the high frequency at which hydrogen interacts with the diamond surface, between each kMC time-step the entire surface will have been subject to a large number of H and  $\text{H}_2$  reactions, such that equilibrium is very rapidly attained. Explicit inclusion of such rapid reactions in the model would dominate the list of executed reaction events, and substantially increase by orders of magnitude the number of kMC events which must be executed.

Making this approximation, a fraction of surface atoms,  $F_{\text{mr}}$ , are activated (*i.e.*, considered to have been converted into monoradical sites) at random at the start of each iteration, based upon the relative rates of H and  $\text{H}_2$  surface reactions under the chosen conditions. From previous work [7]

$$F_{\text{mr}} = \left[ 1 - 0.3 \exp\left(\frac{3430\text{K}}{T_s}\right) + 0.1 \frac{[\text{H}_2]}{[\text{H}]} \exp\left(\frac{-4420\text{K}}{T_s}\right) \right]^{-1} \quad (2)$$

where  $T_s$  is the substrate temperature and  $[\text{H}]$  and  $[\text{H}_2]$  are the near-surface gas-phase concentrations of H and  $\text{H}_2$ , respectively.

## 2.5. Rate list construction

Following random activation of a fraction of the available surface sites at the beginning of a kMC iteration, each surface atom or site is considered for potential surface reaction events, taking into account its state and local environment. Each possible event is stored within the rate list, a 1-dimensional array of all possible reactions, before a weighted rate array (WRA) is constructed. The WRA is a 1-dimensional array of equal length to

the rate list. It represents a cumulative list of rates, providing a means of weighting the probability of a rate being chosen at random by a given event's reaction rate. For example, a reaction which occurs at a speed twice that of another reaction on the surface would have a probability of being chosen that is twice that of the slower rate, due to the reaction occupying a region twice the size in the WRA.

## 2.6. Event execution

Once the randomly chosen reaction event has been identified, that reaction event is executed, followed by any required post-execution tasks. Examples of post-execution tasks include addition or removal of dimer reconstructions, updating the labels for atoms which are now or no longer on the surface, and ensuring that correct hydrogen termination of any affected atoms is maintained. Finally, the simulation time is incremented by the time-step,  $\Delta t$ , completing the iteration.

## 2.7. Specific surface reactions

### 2.7.1. Hydrogen-surface interactions – surface activation and deactivation

Detailed calculations for the migration rates of H across a diamond surface have been recently reported by Guillaume *et al.* [35], but as mentioned earlier, due to the computational expense and difficulty of implementing such rapid processes within a kMC scheme, we chose not to model such interactions explicitly. Instead, we employ a “super-basin approximation” in which a fraction of surface atoms  $F_{\text{mr}}$  (Equation (2)) are activated at random at the start of each iteration, forming surface monoradicals. If an atom is activated, one terminating hydrogen is removed; otherwise, a hydrogen is added, deactivating the carbon.

Possible levels of activation for a given atom are dependent on its bonding to other C atoms and its current activation level, which corresponds to the number of hydrogen atoms implicitly terminating the atom. A  $\text{CH}_2$  surface species with 2 C–C bonds can be activated up to 2 times to create a  $\text{C}_s^{\bullet\bullet}$  radical before it can no longer be activated. A bulk carbon forming 4 C–C bonds is unavailable for activation or deactivation reactions. Currently, no distinction is made between singly and doubly activated carbons, and so they both behave as a surface monoradical.

### 2.7.2. Instantaneous dimer creation

The formation of surface dimers on the {100} surface involves the formation of a  $\text{C}_s\text{--C}_s$  bond between 2 surface carbons, accompanied by a movement of the bonding atoms towards each other. Rather than treating the formation of this bond as an explicit surface reaction, the rapidity of this reaction ( $k \approx 1 \times 10^{12} \text{ s}^{-1}$ ) [23,36]

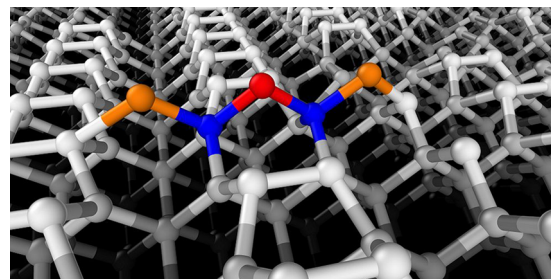


**Figure 2.** When the formation of a dimer between 2 activated adjacent  $\text{C}_s$  atoms (blue) is considered, the red (bridging)  $\text{C}_s$  must be absent, and only one of the two orange  $\text{C}_s$  atoms on either side can be present.

allows us instead to treat dimer formation as instantaneous. During the dimer-creation process, the atoms move towards each other and a bond forms between them. For a dimer to be formed between two adjacent surface carbons, both atoms must be activated and neither can be already part of another dimer reconstruction, there is no carbon bridging both carbons, and collectively they form less than 6  $\text{C}_s\text{--C}_s$  bonds prior to reconstruction (Figure 2).

The requirement that only one  $\text{C}_s$  of the pair can have 3  $\text{C}_s\text{--C}_s$  bonds prior to reconstruction (the orange carbons in Figure 2 represent this 3rd  $\text{C}_s\text{--C}_s$  bond) is two-fold. First, when both participating carbons are bonding to their respective neighbours, the dimer-bond formation requires either the dimer bond or the existing  $\text{C}_s\text{--C}_s$  bonds (the blue-orange bonds in Figure 2) to be stretched, reducing the enthalpy gain from the reconstruction [8]. Second, if such a reconstruction were to occur, the result would be a “saturated dimer,” where both carbons have bulk-like coordination and thus cannot take part in further chemical reactions. Allowing the unlikely formation of these dimers would require the addition of additional dimer-breaking kinetics or growth mechanisms.

### 2.7.3. Dimer breaking

The low energy barrier to the formation of isolated dimers from a surface biradical not only results in very rapid rates of dimer formation, but also of dimer breaking, with the rates of both being  $\sim 1 \times 10^{11} \text{ s}^{-1}$ . However, the local environment of the reconstructing carbons must be taken into account. When the formed dimer is adjacent to an incorporated  $\text{CH}_2$  (Figure 3), although similarly low-energy barriers allow fast reaction rates, in contrast to isolated reconstructions, the formation of these dimers is significantly more reversible. This can be seen by the respective values of their equilibrium constants ( $K_{\text{eq}} = k_f/k_b$ ) being  $K_{\text{eq}} = 6.3$  vs  $K_{\text{eq}} = 4 \times 10^5$  (Table 2, reactions 15 and 17 in Ref. [36]). This difference in  $K_{\text{eq}}$  suggests dimers with adjacent incorporations will exist in equilibrium between dimer bonding and adjacent carbon monoradical structures. From the rates of forming a dimer from two adjacent monoradicals ( $v_f$ ) and of

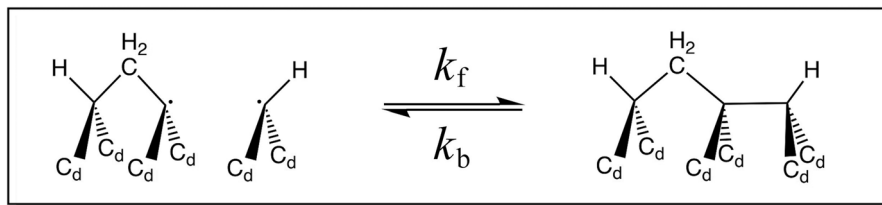


**Figure 3.** The formation and breaking of a dimer reconstruction on the surface from a biradical site when adjacent to a bridging  $\text{CH}_2$  incorporation.

breaking the dimer back to its constituent monoradicals ( $\nu_b$ ), at any point in time, the fraction of dimers with adjacent incorporations which exist as two adjacent monoradicals is approximately given by:

$$F_{\text{broken}} = \frac{\nu_b}{\nu_f + \nu_b} \quad (3)$$

In order to facilitate dimer breaking during the surface-activation process, the implementation of surface activation is updated. In our previous kMC models, activation of the surface and the formation of any possible dimers was carried out in a single step, with activation and assessment of dimer formation occurring in a single consideration of all surface carbons. With dimer breaking turned on, activation of the surface and the formation of dimers are instead decoupled into separate consideration events for the surface atoms, with breaking of dimers with adjacent incorporations included in a 3rd consideration event, if present. As a result, activation of the surface now occurs in the following stages:

1. Activation or deactivation of surface carbons according to the value of  $F_{\text{mr}}$ .
2. Formation of surface dimers between adjacent monoradicals.
3. Breaking of a random number of dimers according to the value of  $F_{\text{broken}}$ .

Results of switching on dimer-breaking are presented in Section 4.3.

#### 2.7.4. Growth species flux

The model employs  $\text{CH}_3$  as the only growth species, at present, because other reactive carbon species ( $\text{CH}_2$ ,  $\text{CH}$ ,  $\text{C}$  and  $\text{C}_2\text{H}$ ) are usually not present in sufficient concentrations at the surface to have a significant effect on growth, contributing less than 1% of total incorporation events [21]. The flux of each growth species at the surface is calculated for each surface site using:

$$F_X = \frac{P_X \bar{c}}{4\rho} [X]_s \quad (4)$$

where  $F_X$  is the per-site flux of a species  $X$ ,  $P_X$  is the species adsorption probability,  $[X]_s$  is the species

concentration at the surface,  $\rho$  is the density of carbon atoms on the (100) diamond surface, and  $\bar{c}$  is the mean speed of the species according to the Maxwell-Boltzmann distribution.

The adsorption probability,  $P_X$ , (also known as the sticking coefficient) is an empirical scaling factor for successful collisions of species  $X$  with the surface, and is a combination of the steric effects of the geometric size and shape of an incident species, spin-state availability, and the accessibility of sites for adsorption. Despite molecular-dynamics attempts to model  $P_X$  [37] for  $X = \text{CH}_3$ , there is little corroborating experimental evidence for the values calculated. This is a serious problem, because  $P_{\text{CH}_3}$  is directly proportional to the calculated growth rate. In future work, all  $P$  factors other than spin-state availability should be implemented on a per-site basis, but for now we have used the same default value as previous models,  $P_{\text{CH}_3} = 0.25$ .

#### 2.7.5. $\text{CH}_x$ incorporation at radical dimer sites

Diamond growth begins through the initial adsorption of a  $\text{CH}_x$  (probably  $\text{CH}_3$ ) species onto a monoradical surface site. The incorporation process of this pendant  $\text{CH}_x$  is then believed to proceed via a ring-opening mechanism first postulated by Garrison *et al.* [38], either at a radical dimer site or trough site [39], as shown in Figure 4.

Because adsorption of a  $\text{CH}_3$  species onto a surface radical (Figure 4(a)) has recently been confirmed theoretically to be barrierless [8], the subsequent incorporation is sufficiently fast under CVD conditions that the rate of incorporation into a radical site can be approximated as the frequency of successful  $\text{CH}_3$  adsorptions,  $F_{\text{CH}_3}$ , calculated using Equation (4). Therefore, the base rate of incorporation of  $\text{CH}_3$ , neglecting any local geometrical or electronic effects, is controlled by surface temperature, the adsorption probability and the concentration of  $\text{CH}_3$  at the surface. Base, per-site rates of  $\text{CH}_3$  incorporation are shown in Table 1.

#### 2.7.6. $\text{CH}_3$ incorporation at trough sites

While the rate of incorporation into both radical dimer surface and trough sites is considered to be rate limited by  $\text{CH}_3$  flux, *ab initio* calculations of  $\text{CH}_3$  incorporation reactions into diamond {100} surfaces [8] indicated that

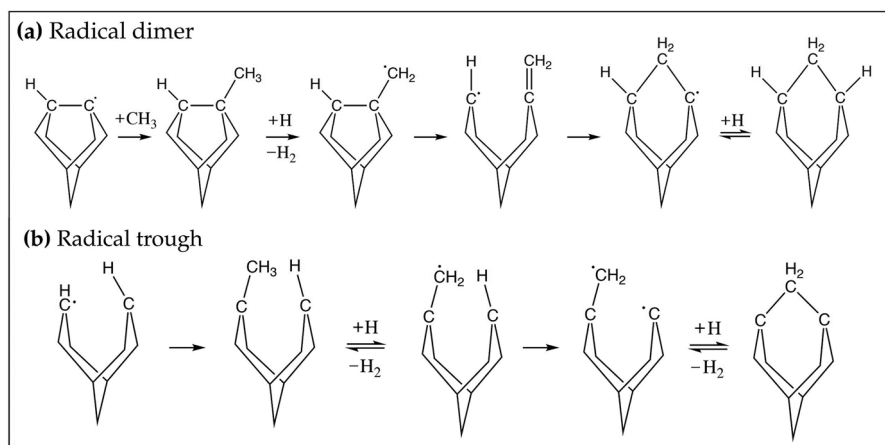


**Figure 4.** The likely  $\text{CH}_3$  incorporation mechanisms via ring-opening following adsorption at (a) radical dimer sites and (b) radical trough sites. (Redrawn based on diagrams in Ref. [8]).

**Table 1.** Rates of  $\text{CH}_3$  incorporation into surface radical sites as a function of growth condition.

Growth condition	SCD (MW)	MCD	NCD	UNCD (HF)	UNCD (MW)
$F_{\text{CH}_3} / \text{s}^{-1}$	179	117	391	127	45

incorporation into trough sites (Figure 4(b)) is more limited due to steric hindrance than originally postulated by Harris & Goodwin [39].

Three distinct trough-site geometries with adsorbed pendant  $\text{CH}_3$  groups are shown in Figure 5: (a) where neither of the adjacent sites are occupied and therefore dimer reconstructions surround the trough site, or where (b) one and (c) two  $\text{CH}_3$  groups, respectively, have incorporated into the adjacent dimer reconstructions. *Ab initio* calculations [8] indicate that the formation of elongated and weak  $\text{C}_s\text{--C}_s$  bonds when incorporation occurs into trough sites with no adjacent atoms (Figure 5(a)) prevents the enthalpy of incorporation from effectively offsetting the loss of entropy due to  $\text{CH}_3$  adsorption, making incorporation unfeasible. However, if both adjacent sites are occupied by  $\text{CH}_2$  species (Figure 5(c)), repulsion by terminating hydrogens is increased and strongly hinders adsorption. Therefore, only after both H atoms have been removed (forming a biradical trough site) can incorporation occur. Finally, when only a single adjacent site is occupied (Figure 5(b)), incorporation is possible at monoradical sites, like dimer radical incorporation.

This approach can be interpreted as kinetic control of trough incorporation, in agreement with assertions by Harris & Goodwin [39] that trough sites are less favourable than dimer radical sites for incorporation. If  $\text{CH}_3$  absorption into “hindered” trough sites (Figure 5(c)) requires two adjacent monoradicals, *i.e.*, a biradical site, where the fraction of biradical sites is:

$$F_{\text{br}} = (F_{\text{mr}})^2 \quad (5)$$

the number of possible trough incorporations is reduced relative to dimer incorporations by local geometry, rather than by increased reaction activation energies. It should be noted that *ab initio* work [8] has so far investigated only the incorporation of  $\text{CH}_3$  species into these sites. It is possible that carbon atoms, which are also thought to be present at the growth surface in non-negligible concentrations under some CVD conditions, and which are significantly smaller than  $\text{CH}_3$  radicals, could incorporate more easily into these sterically hindered sites. This needs to be investigated in future studies.

#### 2.7.7. Migration

Due to the strength of the C–C bond, carbons with more than 2 C–C bonds, including those which form part of a dimer, are not considered for migration. Three modes of migration are considered: Dimer migration, Gap migration, and Migration down step edges.

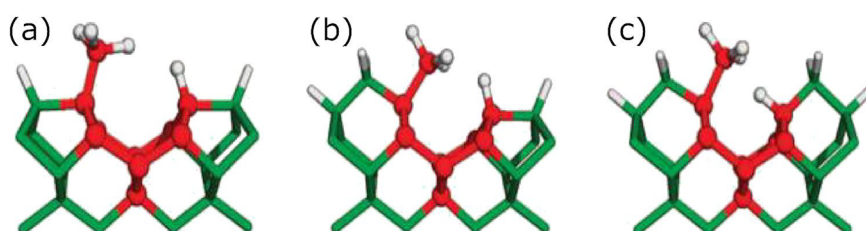


**Figure 5.** Potential trough environments with (a) 2, (b) 1 and (c) zero adjacent dimer reconstructions. (c) The effect of a  $\text{CH}_2$  incorporation on the H atom position; it now sits further into the trough site. Modified from Ref. [40].



**2.7.7.1. Dimer migration.** The scheme for migration of a surface  $\text{CH}_x$  species across the surface between dimer reconstructions in both the chain and row directions (Figure 6) is based on semiempirical calculations [41]. Crucially, migration requires the formation of a biradical trough site between the migrating species and the final migration site. The probability of a biradical site forming,  $F_{\text{br}}$  (Equation (5)) is the product of two monoradicals forming, and so typically only  $\sim 1\%$  of the surface will exist as a biradical at each iteration. The dimer-migration reaction in both chain and row directions exists as a single-step reaction, with the initial breaking of the  $\text{C}_s\text{--C}_s$  bond treated as the rate-limiting-step [41]. A predicted energy barrier of  $E_a = 128 \text{ kJ mol}^{-1}$  suggests rapid reaction rates relative to expected per-site rates of  $\text{CH}_3$  incorporation and hydrogen addition at CVD growth temperatures.

Per-site reaction rates for dimer migration at surface temperatures of 800, 1000 and 1200 K are calculated

using the Arrhenius equation (with  $A = 6.13 \times 10^{13} \text{ s}^{-1}$  [23] and  $E_a = 128.4 \text{ kJ mol}^{-1}$  [41]) to be  $2.5 \times 10^5$ ,  $1.2 \times 10^7$  and  $1.6 \times 10^8 \text{ s}^{-1}$ , respectively.

**2.7.7.2. Gap migration.** The gap-migration or migration-into-gap mechanism has been investigated by Skokov *et al.* [36] using a semi-empirical PM3 cluster model, predicting, similarly to the dimer-migration mechanism, rapid reaction rates under CVD conditions. The proposed family of 4 gap-migration mechanisms (labelled A-D in Figure 7) acts to remove empty trough sites (called “voids” by Netto & Frenklach [23]) through the movement of bridging  $\text{CH}_2$  species into these sites, leaving a new trough site behind. This mechanism for migration was especially important in Netto & Frenklach’s kMC model because only incorporation of  $\text{CH}_3$  into dimer radical sites was considered, and so removal of these voids was essential to enable continuous film growth.

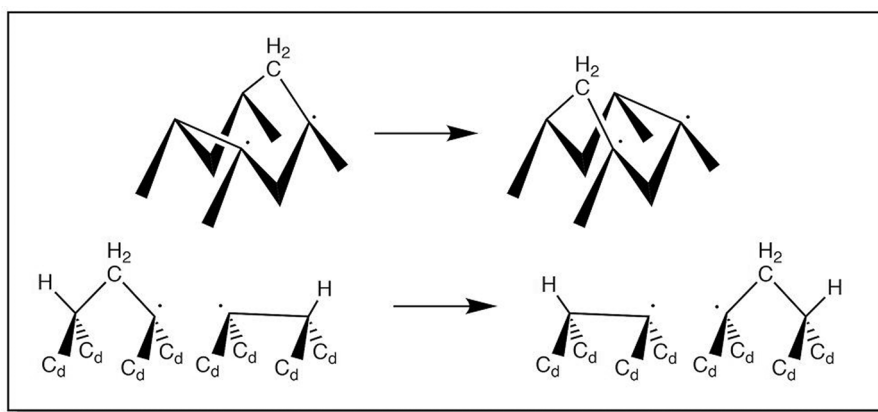


**Figure 6.** Single-step reaction mechanism for the dimer migration of a  $\text{CH}_x$  ( $x=0-2$ ) surface species into an adjacent dimer reconstruction in the dimer row (top) and dimer chain (bottom) directions.  $\text{C}_d$  indicates a bulk carbon that is part of the diamond lattice. The full mechanism can be found in Ref. [23].

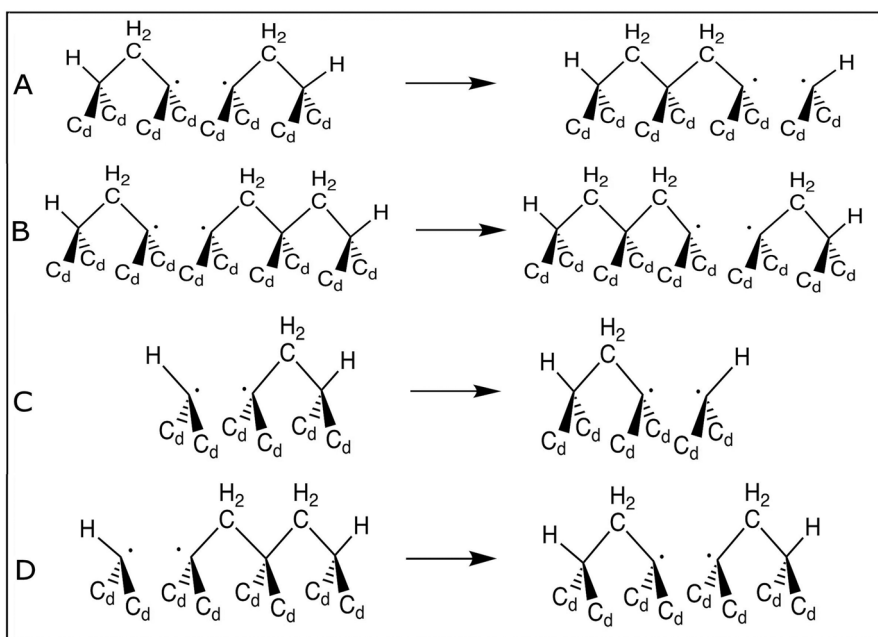


**Figure 7.** The family of gap-migration reactions proposed by Netto & Frenklach [23].

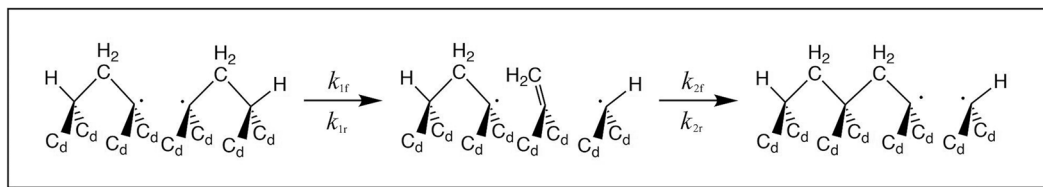


**Figure 8.** Two-step mechanism for type-A gap migration, which is the simplest initial local environment consisting of 2 isolated bridging  $\text{CH}_2$  species separated by a biradical trough.  $\text{C}_d$  indicates a bulk carbon that is part of the diamond lattice.

For simplicity, in our kMC model, each reaction A-D is represented by a single-step reaction rate. To do so, two approximations are made: first, that the steady-state approximation is valid such that each migration pathway can be expressed in terms of the initial structures of A-D only (*i.e.*, those on the left-hand side of Figure 7), and second, that each migration pathway can be generalised by some combination of the type-A sub-reactions, shown in Figure 8.

The application of these approximations produces rate equations shown in (6) to (9), with the rate of each migration type (B–D) expressed in terms of type-A shown in Figure 8.

$$k_A = \frac{k_{1f}k_{2f}}{k_{2f} + k_{2r}} \quad (6)$$

$$k_B = \frac{k_{2f}k_{2r}}{k_{2f} + k_{2r}} \quad (7)$$

$$k_C = \frac{k_{1f}k_{1r}}{k_{1r} + k_{1r}} \quad (8)$$

$$k_D = \frac{k_{1r}k_{2r}}{k_{2f} + k_{1r}} \quad (9)$$

Once the rate for each sub-reaction has been calculated (Table S2 in the Supplementary Information), the single-step reaction rate for each migration type can be determined. As seen in Table 2, these migration reactions are highly temperature dependent. At lower CVD growth temperatures, migrations occur at comparable rates to those for incorporation (Table 1), but at higher temperatures migrations become significantly faster than incorporation events. Due to the specific local geometries required, there is no direct competition between the reactions, with the exception of reactions A and D, which represent opposite movements of a  $\text{CH}_x$  species.

**2.7.7.3. Migration down an atomic step.** Calculations by Richley *et al.* [42] suggested that under CVD conditions, the migration of  $\text{CH}_2$  species down atomic {111} steps on {100} surfaces could be considered as facile as lateral migrations. The rate of migration down an atomic step, therefore, is calculated using the same Arrhenius reaction rate as for dimer migration. Similar

to the other migration implementations, our down-migration implementation requires (a) an atomic step, (b) specific terminating hydrogen atoms to be removed, and (c) the geometry of the final atomic site to be suitable for supporting the migrating carbon.

The implemented preliminary 1-step reaction for this migration is shown in Figure 9, where the activation and geometrical conditions can be seen. With respect to monoradicals, the terminating hydrogen between the migrating  $\text{CH}_2$  species (shown by the blue arrow) and the final site must be absent (red arrow) as well as one of the carbons supporting the migration species at its final site, allowing an initial  $\text{C}_s\text{--C}_s$  bond to be formed. Finally, *both* atoms supporting the final position of the migrating carbon must be present, consistent with the current implementation of  $\text{CH}_x$  incorporation. The presence of a dimer bond between the supporting carbons is not checked, as in either case, once a  $\text{C}_s\text{--C}_s$  bond has formed between the supporting and migrating carbons the resulting incorporation is approximated as an incorporation into a trough or dimer site.

The inclusion of this down-migration mechanism is likely to have two effects: reduction in the likelihood of etching for  $\text{CH}_x$  species isolated on higher atomic layers because they now can escape to lower levels where they are less exposed, and smoothing of the growth surface as migrating  $\text{CH}_x$  species extend lower-level terraces and fill voids in the surface. However, similar to other migration pathways, the dependence on monoradical distribution can limit execution of these reactions.

It is worth noting that the model currently treats step-edge atoms as geometrically ideal and chemically equivalent to flat terrace atoms, following the work in Ref. [42]. In reality, however, step-edge atoms can exhibit lower coordination, local strain, or altered hydrogen termination, which can significantly affect chemical processes occurring there, in particular,  $\text{CH}_x$  insertion, H abstraction, or dimer formation. Before such modified processes can be incorporated into a kMC simulation such as this, the behaviour and geometries of step-edge

**Table 2.** Reaction rates,  $\nu$  (in  $\text{s}^{-1}$ ), for overall gap-migration rates (A–D) at surface temperatures of 800, 1000 and 1200 K, calculated using Eqs. (6)–(9) and values from Table S2.

Reaction	$\nu_{800\text{ K}}$	$\nu_{1000\text{ K}}$	$\nu_{1200\text{ K}}$
A	$7.4 \times 10^3$	$7.1 \times 10^5$	$1.5 \times 10^7$
B	$7.4 \times 10^4$	$3.9 \times 10^6$	$5.5 \times 10^7$
C	$1.2 \times 10^1$	$3.7 \times 10^3$	$1.7 \times 10^5$
D	$4.9 \times 10^2$	$8.1 \times 10^4$	$2.4 \times 10^6$

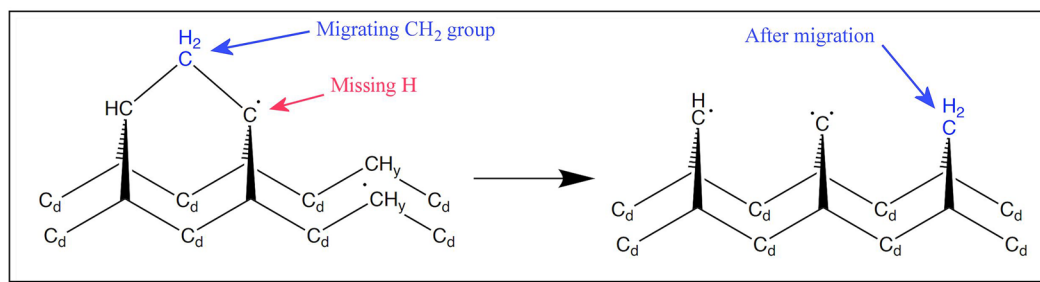


**Figure 9.** Single-step mechanism for the migration of a  $\text{CH}_2$  species (blue) down an atomic step. The migrating species must be a bridging group, forming only 2  $\text{C}_s\text{--C}_s$  bonds.

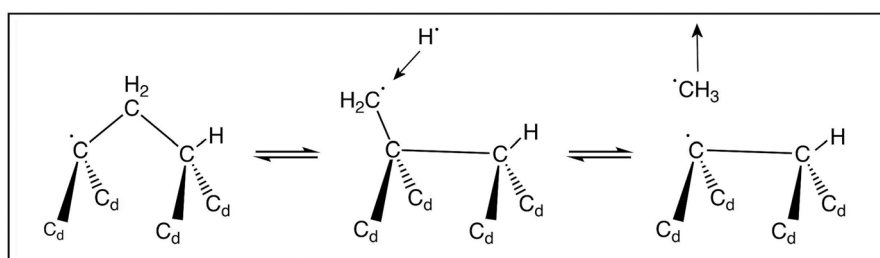


**Figure 10.** Mechanism for etching of a  $\text{CH}_2$  species previously incorporated into a dimer radical site, operating as a direct reverse of the incorporation process.

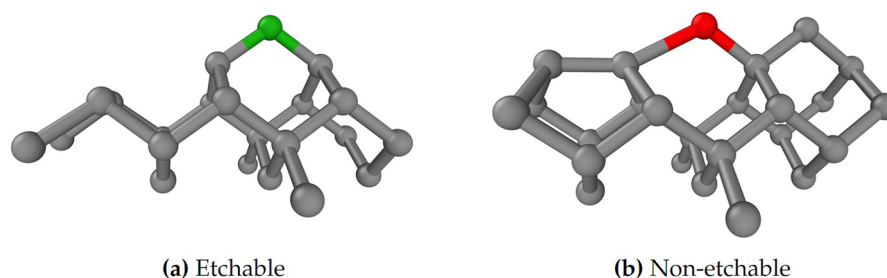


**Figure 11.** Etchable (green) and non-etchable (red) atoms according to the Battaile *et al.* preferential-etching model [28]. (a) A  $\text{C}_s$  atom isolated along the SA direction is rapidly etched, while (b)  $\text{C}_s$  atoms that form part of an SA step-edge are considered non-etchable.

atoms need to be better understood. We would encourage enthusiastic readers to attempt high-level DFT-type calculations of step-edge atoms to expedite this process.

### 2.7.8. Etching

Results from quantum-mechanical modelling of small {100} surface clusters [28,43] suggested that not only was incorporation into monoradical dimer reconstructions (Sections 2.7.5 and 2.7.6) reversible with a small change in Gibbs energy, but that such reactions would be relatively fast under CVD growth conditions. The proposed mechanism, which involves the reformation of the dimer reconstruction, is shown in Figure 10, following the abstraction of a terminating hydrogen.

The reversible nature of the reaction originates from the reformation of the dimer during the etching process. Therefore, etching is only rapid when the local environment of a target carbon allows such a reconstruction to occur, such as when the carbon has no adjacent carbons along the chain direction and is therefore “isolated”. As described in Section 2.7.3, a carbon with 3  $\text{C}_s\text{--C}_s$  bonds can still reconstruct to form a

dimer, as included in other models [23]. However, when this occurs, the elongation of the existing  $\text{C}_s\text{--C}_s$  bond reduces the enthalpy gained through dimer formation, with quantum-mechanical modelling suggesting that the Gibbs energy of the overall etching reaction becomes endothermic when the carbon is not “isolated” [28,43]. The transition from an exothermic to endothermic etching mechanism limits the etching of carbons by this mechanism to those considered “isolated,” described below.

Whether a carbon can be considered “isolated” or not is determined by considering the neighbouring atoms bonded to the carbon in question, although this can be generalised to identifying step-edge environments. Using the nomenclature of Battaile *et al.* [28], a carbon forming a type-A step-edge (SB) or isolated along the SB direction (Figure 11(a)) and not part of a {100} chain, is considered etchable. Figure 11(b) shows how the incorporation of a single adjacent atom to an initially isolated surface atom prevents preferential etching of the central surface, reducing the ability of the resulting structure to reconstruct.

**Table 3.** Rates of preferential etching and the ratio of etching-to-incorporation rates for four of the growth conditions described in section 2.2.

Growth condition	$T_s / \text{K}$	$[\text{H}] / \text{cm}^{-3}$	$v_{\text{etch}} / \text{s}^{-1}$	$v_{\text{etch}} : v_{\text{incorp}}$
SCD	973	$3.4 \times 10^{16}$	$6.9 \times 10^5$	3834
MCD	1173	$1.85 \times 10^{14}$	$7.5 \times 10^3$	63
NCD	1173	$1.52 \times 10^{14}$	$6.2 \times 10^3$	16
UNCD (HF)	1173	$3.0 \times 10^{13}$	$1.2 \times 10^3$	9.4

Etching rates were calculated using  $v = k[\text{H}] = A \exp(-E_a/RT_s)[\text{H}]$ .

Calculations were also carried out for carbons with one or two adjacent incorporations (Figure 11(b)), finding that the etching of “non-isolated” carbons was endothermic and therefore not likely to occur at significant rates. Therefore, only surface carbons which have no incorporations into adjacent trough sites are considered to be etchable [28].

Depending on the growth conditions, while only a small proportion of the surface carbons are considered for etching during each iteration, a rapid rate of etching ensures that the probability of these reactions being chosen is much greater than those for individual  $\text{CH}_x$  incorporation reactions. Using an energy barrier of  $E_{\text{etch}} = 32.7 \text{ kJ mol}^{-1}$  and Arrhenius pre-exponential factor of  $7 \times 10^{14} \text{ s}^{-1}$  [28], the rates of etching are shown in Table 3. Rates of etching are very rapid relative to incorporation, except under conditions with low atomic-hydrogen concentrations or low surface temperatures. When rates of etching relative to incorporation are high, extreme smoothing of the surface is expected due to limited incorporation away from step-edges, while at lower rates of etching, rougher morphologies might occur due to incorporation at increasingly random locations. As etching is fast for C atoms considered “isolated” but otherwise zero, this is referred to as a preferential-etching model [28].

However, this energy barrier to isolated etching ( $E_{\text{etch}}$ ) is based on calculations carried out over 20 years ago [8,28,43] using quantum-mechanical PM3 methods which have the tendency to underestimate C–C bond strengths [8]. Therefore, this energy barrier is likely to be an underestimate, but nevertheless provides a useful starting point.

Another possible carbon-loss mechanism involves the removal of pendant hydrocarbon chains from the surface through  $\beta$ -scission reactions, named after the breaking of the  $\beta$ -bond between the first and second carbons from the dehydrogenated carbon. This leads to rapid loss of ethene ( $\text{C}_2\text{H}_4$ ) or methyl back into the gas phase preventing longer hydrocarbon chains from forming, which might otherwise cross-link on the surface and create surface defects [9]. Because previous kMC models found that the effects of  $\beta$ -scission processes on growth rates and surface morphologies were generally limited [21], in the current model, these reactions were not modelled explicitly. Instead, the reaction rate of  $\beta$ -scission is implicitly treated to be infinitely fast, preventing the formation of any  $\text{C}_x\text{H}_y$  chains.

## 2.8. Growth simulations

A growth simulation represents a sequence of surface reactions from a pristine,  $\{100\}:\text{H}$ ,  $2 \times 1$  reconstructed diamond surface (Section 2.1) until a chosen end-point is reached. A simulation is often identified by the growth conditions which represent the majority of the simulation growth parameters, such as MCD, SCD or UNCD, as outlined in Section 2.2. The point at which a simulation terminates is controlled by either simulation time, average growth-height or total kMC iterations, depending on the end-point that is reached first. The choice of termination method can affect the final simulation geometries. Some surface features, such as pits, step-edges, hillocks, defect formation, *etc.*, take time to develop in the simulation, and so terminating the growth process too early may prevent these features being seen. Conversely, running the simulation for too long may allow some of these features to be overgrown and buried beneath the encroaching flat surface. So, when comparing different growth parameters, the same termination method (time, growth height, or iterations) was used to ensure comparing like with like.

## 3. Simulation visualisation

An important part of the computational implementation is the ability to visualise the growing surface at the atomic level over the course of the simulation. The surface state can be output periodically in extended-xyz format, allowing the current surface state (carbon positions, activation, reconstruction) following a reaction event to be visualised in a suitable viewer, such as OVITO [44] (Figure 12).

## 4. Model predictions

### 4.1. Growth-rate and roughness predictions

We now compare our model predictions with theoretical predictions and experiment. Growth-rate and final roughness predictions for different types of diamond growth are shown in Table 4.

With the exception of SCD growth conditions, our model is in reasonable agreement with both experimental predictions and previous cubic kMC simulations. Roughness values, while higher than those from the previous cubic model, follow the same hierarchical trend expected experimentally: *i.e.*, that SCD, MCD, NCD and UNCD growth conditions produce increasingly rougher surfaces.

However, under SCD growth conditions, a large disparity in growth-rate predictions exists between our model and previous work [21] being significantly slower than the experimental growth rate of several  $\mu\text{m h}^{-1}$ . This discrepancy could be due to the role of other hydrocarbons, particularly atomic carbon, being underestimated in SCD MW plasmas and these species



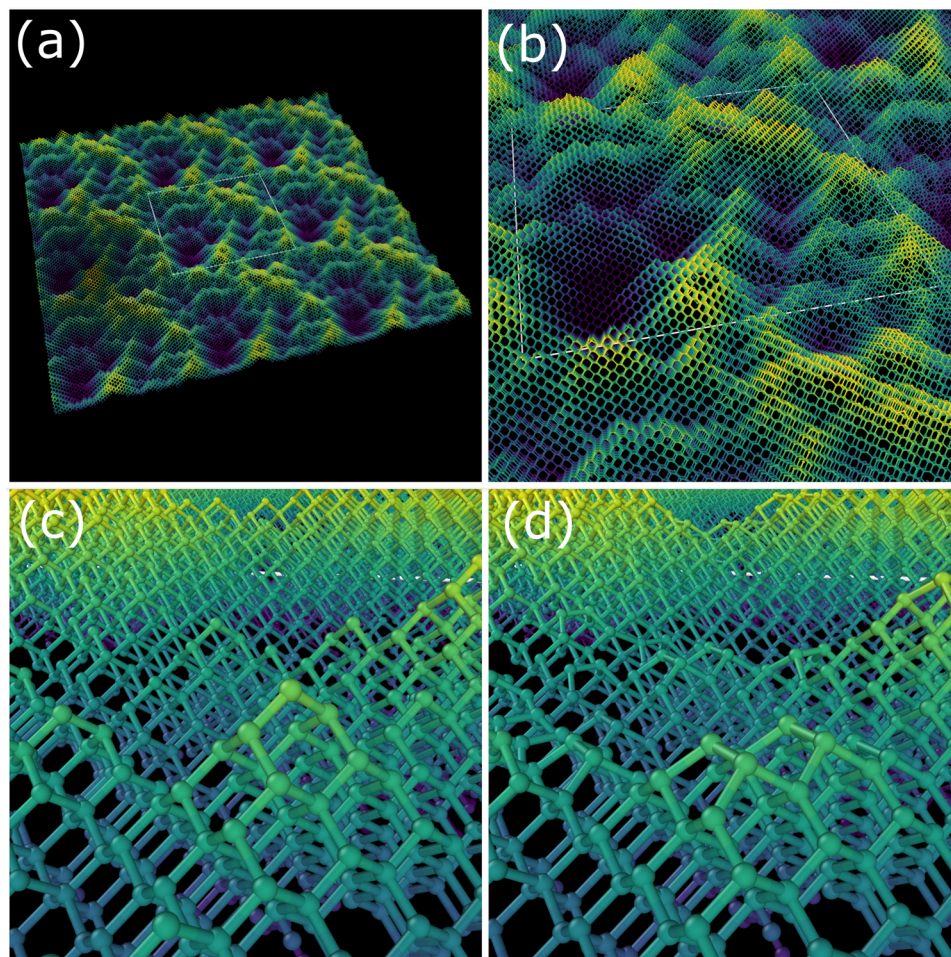


**Figure 12.** Available atomic-level visualisation, increasing in magnification from (a) to (c), and (d) showing a slightly rotated view of (c). Extended xyz frames are visualised using the software tool OVITO [44]. To aid visualisation, the surface is replicated along its periodic boundaries; the original surface dimensions are indicated by a white outline, with false-colouring used to help distinguish the vertical height of atoms and surface features.

**Table 4.** Experimental (exp.) and kMC simulated (kMC) growth rates ( $G$ ) and final r.m.s. roughness values ( $R$ ) for MCD, NCD, SCD, UNCD growth conditions in hot-filament (HF) or microwave plasma (MW) reactors.

Growth condition (reactor type)	MCD (HF)	NCD (HF)	SCD (MW)	UNCD (HF)	UNCD (MW)	Ref.
$G$ (exp.)/(nm h <sup>-1</sup> )	350	1000	3000–4000	60	100	[30]
$G$ (kMC)/(nm h <sup>-1</sup> )	390	2300	533	68	–	[21]
$G$ (kMC)/(nm h <sup>-1</sup> )	$437 \pm 13$	$1261 \pm 31$	$85 \pm 3$	$93 \pm 2$	$49 \pm 1$	[This work]
$R$ (kMC)/nm	0.077	0.086	0.057	0.12	–	[21]
$R$ (kMC)/nm	0.60	0.51	0.04	0.38	0.053	[This work]

3D cubic simulations [21] used species concentrations at 0.5 mm above the surface with no extrapolation, while this work utilises extrapolation of concentration to the surface (Section 2.2). Growth rates and roughness values from this work represent averages of 10 simulation sets, which were each grown to 120 Å.

play as-yet unmodelled key roles under these growth conditions. This would be an important focus of future investigations, both theoretically and experimentally.

Predictions of growth rates and film roughness as a function of growth conditions, such as CH<sub>3</sub> concentration, substrate temperature, migration, and many other growth parameters were found to be largely in agreement with those of the previous cubic model [21]. Therefore, there is no need to repeat these results again here; the reader is pointed towards Ref. [25] if they wish to see these results in detail. Instead, we shall focus upon the predictions of the new additions to the growth model, especially migration pathways, and dimer making/breaking reactions.

#### 4.2. Effect of migration

The three distinct modes of migration, dimer migration, gap migration and migration down atomic steps, described in Section 2.7.7, can be included in the growth model independently. For each combination of migration pathway included in the growth model, sets of 20 simulations were created using SCD and MCD growth conditions until an average height of 120 Å was reached.

First, considering MCD conditions (Figure 13), the effects on growth-rate and roughness values are largely migration-scheme dependent, although migration down atomic steps showed the most significant effect. We find that when all three migration pathways are included, they operate synchronously, allowing surface species to

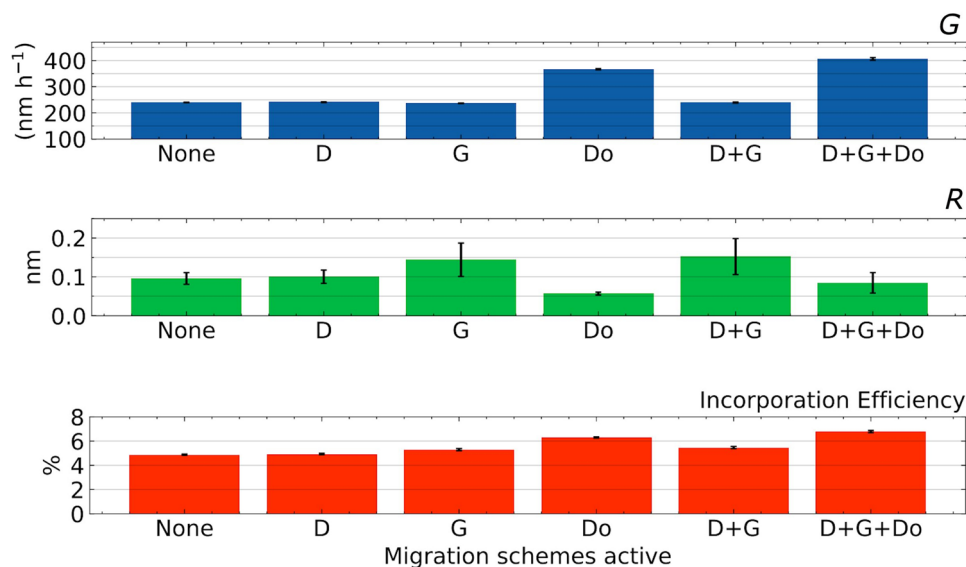


**Figure 13.** Effect on growth rate ( $G$ ), r.m.s. roughness ( $R$ ), and incorporation efficiency (percentage incorporation events – percentage etching events) when migration is introduced into the growth model. Each bar and the corresponding error represent sample averages and standard deviations for a set of 20 simulations, grown to 120 Å under MCD growth conditions for 6 migration-scheme combinations: No migration (None), dimer only (D), gap only (G), down only (Do), D + G and D + G + Do (all).

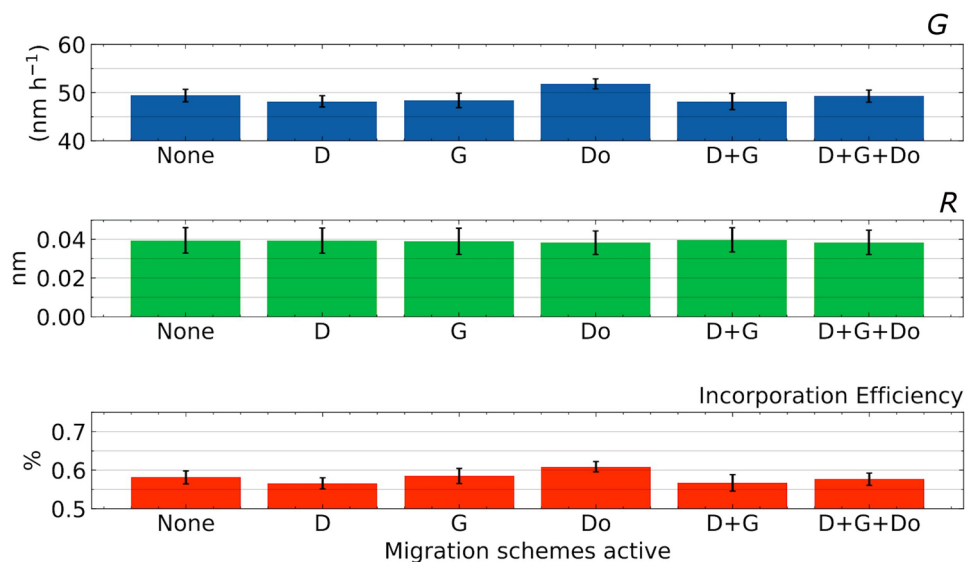


**Figure 14.** Effect on growth rate ( $G$ ), r.m.s. roughness ( $R$ ), and incorporation efficiency (percentage incorporation events – percentage etching events) when migration is introduced into the growth model. Each bar and the corresponding error represent sample averages and standard deviations for a set of 20 simulations, grown to 60 Å under SCD growth conditions for 6 migration-scheme combinations: No migration (None), dimer only (D), gap only (G), down only (Do), D + G and D + G + Do (all).

be stabilised against etching, either through the formation of a stable growth nucleus in the same atomic layer, or, due to migration down a step-edge, to be stabilised in the layer below. Thus, growth rate is significantly increased although roughness is barely changed.

The inclusion of gap-migration increases roughness, suggesting that while gap migration operates over shorter length-scales relative to dimer migration, it can also affect morphology over a larger scale. The gap-migration mechanism primarily acts to consolidate surface terraces, effectively moving hindered trough sites (which require creation of a biradical to incorporate  $\text{CH}_x$ ) across the surface. By encouraging formation of more complete surface terraces, gap-migration reactions

increase support for incorporation of species into the layer above, nucleating new growth layers. The nucleation of new layers at the expense of layer-by-layer growth, similar to island growth, increases roughness.

Considering incorporation efficiency, increases to roughness values when down-migration is included can be directly linked to the increase in net incorporation. Bridging carbon species can migrate rapidly to a stable site in the layer below before they can be etched away.

Conversely, for SCD conditions (Figure 14), the effect of migration is much less pronounced. Growth rate is largely unchanged by the introduction of migration reactions. Down-migration, similar to MCD growth conditions, increases incorporation efficiency slightly by



allowing isolated species to migrate to stable sites in the atomic layer below. However, this increase in incorporation is limited by the availability of these type of migrations, representing just 0.20% of all events, due to lower concentrations of monoradical sites and a lower migration reaction rate. Overall migration is also reduced relative to MCD conditions, with just 3.5% of events representing migrations compared to 25% of events under MCD growth conditions.

### 4.3. Effect of dimer breaking

As outlined in Section 2.7.3, the relative rates of dimer formation and breaking suggest that for dimers which have a bridging  $\text{CH}_x$  species adjacent (Figure 3), at a given moment a fraction of these dimers will instead exist on the surface as two adjacent carbon monoradicals. The percentage of dimers which exist in a “broken,” biradical state at any instant, along with the reaction rates for dimer formation and breaking for MCD and NCD growth conditions, are shown in Table 5.

Dimer creation is inherent to the kMC model, but dimer breaking is optional and can be switched on or off to investigate its effects upon the simulation. When dimer breaking was introduced into the model using the values in Table 5 under MCD and NCD growth conditions, the growth rate increased by 25%. However, no significant change in growth rate or roughness was seen under SCD conditions due to the small proportion of dimers broken each iteration. The roughness was strongly reduced by dimer breaking, as shown in Figure 15(a,b), the formation of pits prevents a significant reduction in roughness on the length-scale of the surface. However, as shown by the large, smooth terraces present in Figure 15(b), the randomised breaking of dimers has a remarkable smoothing effect upon the median surface-roughness of films grown under MCD growth conditions. The presence of increased numbers of biradicals from broken dimers reduces the formation frequency of the pits shown in Figure 15(a) which are largely absent in Figure 15(b).

These changes to growth rates and surface morphologies under MCD and NCD growth conditions are driven by gap-migration events, primarily type-C gap migrations (recall Figure 7). When dimer breaking is

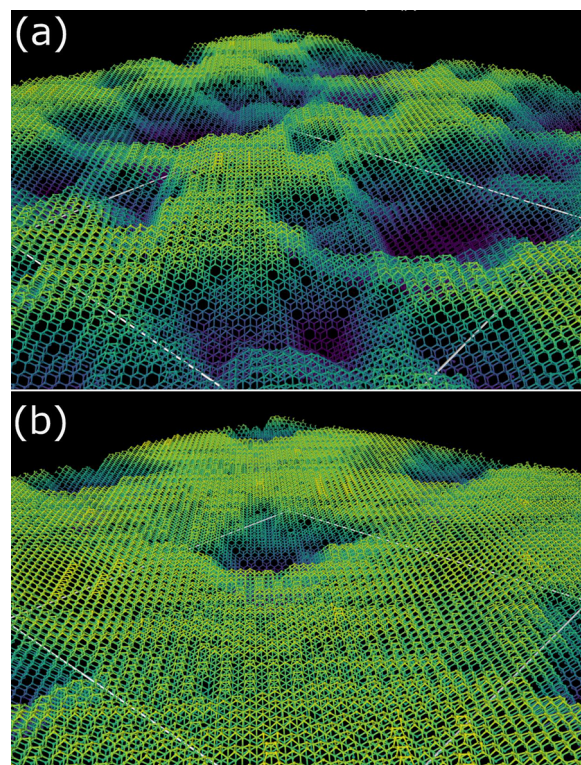


**Figure 15.** Median surfaces by surface roughness after 120 Å growth under MCD growth conditions with (a) dimer breaking inactive, and (b) dimer breaking active.

activated, calculations show that type-C gap-migration events increase from 0.6% of total events to 2.4%, and from 0.5 to 3.2%, for MCD and NCD growth conditions, respectively. Dimer breaking strongly affects the possibility of gap migration due to its reliance on adjacent monoradicals, which are otherwise blocked by the presence of a dimer. If the rapidity of dimer-breaking reactions allows them to occur during the gap-migration process, such that a dimer is treated as two adjacent monoradicals, gap-migration reactions dominate the simulations. Our recommendation, therefore, is to keep dimer-breaking switched on in all subsequent simulations.

## 5. Conclusions

In this paper we have described the implementation of an updated kMC code to simulate CVD diamond growth using a full 3D tetrahedral structure for diamond. The implemented growth model can simulate minutes of growth for systems of more than 10,000 carbons, and is parametrised by growth-condition inputs taken from detailed modelling and experiment. Predictions of growth rates and film roughness over a wide range of growth conditions were largely in agreement with experimental literature and previous simulations. The model suggests that surface migration plays an important role for MCD and NCD growth conditions, increasing growth rates significantly although not substantially affecting roughness. Under SCD conditions, migration

**Table 5.** Reaction rates for the formation ( $v_f$ ) and breaking ( $v_b$ ) of dimers with adjacent  $\text{CH}_x$  incorporations at different substrate temperatures,  $T_s$ , under MCD and SCD growth conditions

Condition	MCD (HF)	SCD (MW)
$T_s/\text{K}$	1167	973
$v_f/\text{s}^{-1}$	$7.4 \times 10^{11}$	$7.0 \times 10^{11}$
$v_b/\text{s}^{-1}$	$1.0 \times 10^{11}$	$3.0 \times 10^{10}$
$F_{\text{broken}}$	12.3%	4.1%

Reaction rates are calculated from an Arrhenius expression using activation energies and pre-exponential factors for dimer formation ( $2.9 \text{ kJ mol}^{-1}$ ,  $10^{12} \text{ s}^{-1}$ ) and breaking ( $59.8 \text{ kJ mol}^{-1}$ ,  $4.79 \times 10^{13} \text{ s}^{-1}$ ), respectively, given by Netto & Frenklach [23]. The proportion of dimers which exist in a broken, biradical state ( $F_{\text{broken}}$ ) is calculated from Equation (3).

events are relatively less common and so play a much smaller role in growth. Nevertheless, we recommend that the three migration events added to the model, dimer migration, gap migration and migration down atomic steps, are key processes occurring on the diamond surface during growth and should be included in any future simulations.

Using a realistic tetrahedral structure in our new model enables growth mechanisms to be simulated and tested for viability that were not previously possible in less sophisticated models. Two such mechanisms evaluated were dimer creation and dimer breaking. The inclusion of either one of these mechanisms individually had little effect upon growth rates or roughness. However, the inclusion of both mechanisms simultaneously significantly increased growth rates by a factor of almost 2, and decreased roughness by ~10% for NCD and MCD conditions. These changes to growth rates and surface morphologies are driven by increased type-C gap-migration events. We conclude that if accurate values for the growth rate and roughness are required, it is necessary to include both these dimer-making and breaking events in any kMC subsequent models of the growing diamond surface.

Other mechanisms involving dimer reconstruction have yet to be included in the model, and may make the growth simulation even more accurate. These include etching of isolated dimers, and preferential dimer alignment into rows. Underlying processes producing aligned dimer structures fall into two categories: passive and active alignment. Passive alignment processes encompass situations where the energetics of aligned and misaligned geometries encourage alignment of dimers when possible. Active alignment processes require chemical reactions, preferentially breaking misaligned dimers or certain migration and incorporation pathways which encourage dimer alignment. The addition of these processes to the model and their effects upon diamond growth would make valuable future additions to the model.

Still missing from the model are the roles of potential growth species other than  $\text{CH}_3$ , in particular C atoms,  $\text{C}_2$  and  $\text{C}_2\text{H}$ , which can have non-negligible concentration under certain growth conditions, *e.g.*, those for SCD or UNCD. Addition of mechanisms for these species to add to or insert into the diamond lattice might prove to be a powerful route to simulate the formation of defects, such as dislocations, or the renucleation processes responsible for the formation of polycrystalline films. A realistic 3D tetrahedral model of the diamond surface now makes these more complex simulations possible, and will be an obvious extension of this work. However, choice of suitable values for the adsorption probability,  $P_x$ , for each of these species is not trivial. Furthermore, the current model treats the adsorption of all  $\text{CH}_x$  ( $x=0-3$ ) species independently. But under high carbon flux or hydrogen-deficient conditions, co-adsorption

effects, such as transient clustering, site blocking, or cooperative adsorption, may influence incorporation rates and surface migration, and so may need to be added to the model for improved accuracy.

Another important factor is that only  $sp^3$ -carbon-forming surface reactions are considered at present. For true simulation of defect formation, a model for  $sp^2$ -carbon growth and etching is also required.

Another mechanism still to be added explicitly to the model is  $\beta$ -scission, with the  $\beta$ -scission reaction rate currently being implicitly treated as infinitely fast. Previous kMC models found that the effects of  $\beta$ -scission on growth rates and surface morphologies were generally limited [21]. Nevertheless, now with a realistic structural model, inclusion of a proper model for  $\beta$ -scission might provide some further insight into growth behaviour.

Overall, we believe this simulation platform and implemented growth model offers powerful atomic-scale analysis and enables investigation of a range of potential mechanisms that affect diamond CVD. As well as defect formation, future studies will include growth enhancement facilitated by the introduction of N-containing species, doping by B and P, and even the formation of NV centres.

## Acknowledgements

MDGW wishes to thank the UK EPSRC via the UK EPSRC Centre for Doctoral Training in Diamond Science & Technology, and Ila Technologies, Ltd for joint funding. This work was carried out using the computational facilities of the Advanced Computing Research Centre, University of Bristol (<http://bris.ac.uk/acrc/>).

## Disclosure statement

No potential conflict of interest was reported by the author(s).

## Funding

This work was supported by Engineering and Physical Sciences Research Council [grant EP/L015315/1]; Ila Technologies, Ltd (Singapore).

## Notes on contributors

**Dr Max Williams** studied Chemical Physics at Bristol University and then stayed on to do a PhD in the CVD Diamond group supervised by Profs May and Allan. His PhD project involved upgrading the previous kMC growth model using a more realistic tetrahedral model for the diamond surface, and this paper is based on the work in his thesis. He is currently a software engineer for a commercial company.

**Professor Paul May** studied Chemistry at Bristol University (1982-85). After 3 years working in the semiconductor industry, he returned to Bristol to do his PhD in the area of plasma etching. He graduated in 1991, and co-founded the CVD diamond group at Bristol with colleague Prof Mike Ashfold FRS. He later won a Ramsay Memorial Fellowship, then a Royal Society University Research Fellowship, which allowed him



to expand the Bristol diamond activities into a self-contained research group within the department. Paul was promoted to Professor in August 2009. The Bristol CVD diamond group now has several academic staff associated with it, around 8 PhD students, 2 postdocs and almost £4M of equipment, making it one of the largest university diamond research groups in the UK. Paul's research area focuses upon CVD diamond and he has published nearly 250 scientific papers in peer-reviewed Journals, along with several book chapters.

**Professor Neil Allan** is a professor of Physical Chemistry at Bristol (since 2003), a former Director of the Centre of Computational Chemistry there (2008–2011), and from 2015–2019 was the Chair of the UK Collaborative Project for the Simulation of Condensed Matter (CCP5). He did his DPhil at Oxford University and then spent four years working at ICI, before moving to Bristol in 1989. He has forty years' experience in computational chemistry and molecular modelling in materials of technological, industrial and geological interest, using a wide variety of theoretical techniques, ranging from atomistic lattice simulations to *ab initio* electronic structure calculations. New structures have been predicted, such as a graphene structure for zinc oxide, subsequently characterised experimentally. He has long-standing interests in defect thermodynamics, non-stoichiometry and solid solutions, and has collaborated extensively with Paul May for many years. He is a former Royal Society of Chemistry prize winner for Geochemistry.

## ORCID

Paul W. May  <http://orcid.org/0000-0002-5190-7847>

Neil L. Allan  <http://orcid.org/0000-0001-9342-6198>

## References

- [1] May PW. Diamond thin films: a 21st century material. *Phil Trans R Soc Lond A*. 2000;358(1766):473–495. doi: [10.1098/rsta.2000.0542](https://doi.org/10.1098/rsta.2000.0542)
- [2] Zulkharnay R, May PW. Applications of diamond films: a review. *Funct Diamond*. 2024;4:2410160. doi: [10.1080/26941112.2024.2410160](https://doi.org/10.1080/26941112.2024.2410160)
- [3] Tallaire A, Achard J, Silva F, et al. Growth of large size diamond single crystals by plasma assisted chemical vapour deposition: recent achievements and remaining challenges. *Comptes Rendus Physique*. 2013;14(2–3):169–184. doi: [10.1016/j.crhy.2012.10.008](https://doi.org/10.1016/j.crhy.2012.10.008)
- [4] May PW, Zulkharnay R. Diamond thin films: a 21st century material. Part 2: a new hope. *Phil Trans Roy Soc Lond A*. 2024;383:20230382. doi: [10.1098/rsta.2023-0382](https://doi.org/10.1098/rsta.2023-0382)
- [5] Ashfold MNR, May PW, Petherbridge JR, et al. Unravelling aspects of the gas phase chemistry involved in diamond chemical vapour deposition. *Phys Chem Chem Phys*. 2001;3(17):3471–3485. doi: [10.1039/B104265N](https://doi.org/10.1039/B104265N)
- [6] Goodwin DG, Butler JE. Handbook of industrial diamonds and diamond films. Prelas MA, Popovici G, Bigelow LK, editors. New York: Marcel Dekker; 1998.
- [7] May PW, Mankelevich YA. Experiment and modeling of the deposition of ultrananocrystalline diamond films using hot filament chemical vapor deposition and Ar/CH<sub>4</sub>/H<sub>2</sub> gas mixtures: a generalized mechanism for ultrananocrystalline diamond growth. *J Appl Phys*. 2006;100:024301. doi: [10.1063/1.2214304](https://doi.org/10.1063/1.2214304)
- [8] Cheesman A, Harvey JN, Ashfold MN. Studies of carbon incorporation on the diamond {100} surface during chemical vapor deposition using density functional theory. *J Phys Chem A*. 2008;112(45):11436–11448. doi: [10.1021/jp8034538](https://doi.org/10.1021/jp8034538)
- [9] Butler JE, Woodin RL, Brown LM, et al. Thin film diamond growth mechanisms. *Philos Trans R Soc A Math Phys Eng Sci*. 1993;342:209–224. doi: [10.1098/rsta.1993.0015](https://doi.org/10.1098/rsta.1993.0015)
- [10] Harris SJ. Mechanism for diamond growth from methyl radicals. *Appl Phys Lett*. 1990;56(23):2298–2300. doi: [10.1063/1.102946](https://doi.org/10.1063/1.102946)
- [11] Larsson K. Adsorption of hydrocarbon species on a stepped diamond (111) surface. *Phys Rev B*. 1997;56(23):15452–15458. doi: [10.1103/PhysRevB.56.15452](https://doi.org/10.1103/PhysRevB.56.15452)
- [12] Levi AC, Kotrla M. Theory and simulation of crystal growth. *J Phys Condens Matter*. 1997;9(2):299–344. doi: [10.1088/0953-8984/9/2/001](https://doi.org/10.1088/0953-8984/9/2/001)
- [13] Pineda M, Stamatakis M. Kinetic Monte Carlo simulations for heterogeneous catalysis: fundamentals, current status, and challenges. *J Chem Phys*. 2022;156(12):120902. doi: [10.1063/5.0083251](https://doi.org/10.1063/5.0083251)
- [14] May PW, Allan NL, Richley JC, et al. Simplified Monte Carlo simulations of CVD diamond growth. *J Phys Condens Matter*. 2009;21(36):364203. doi: [10.1088/0953-8984/21/36/364203](https://doi.org/10.1088/0953-8984/21/36/364203)
- [15] May PW, Allan NL, Ashfold MNR, et al. Simulations of polycrystalline CVD diamond film growth using a simplified Monte Carlo model. *Diamond Relat Mater*. 2010;19(5–6):389–396. doi: [10.1016/j.diamond.2009.10.030](https://doi.org/10.1016/j.diamond.2009.10.030)
- [16] May PW, Harvey JN, Allan NL, et al. Simulations of CVD diamond film growth using a kinetic Monte Carlo model. *J Appl Phys*. 2010;108:014905. doi: [10.1063/1.3437647](https://doi.org/10.1063/1.3437647)
- [17] May PW, Harvey JN, Allan NL, et al. Simulations of chemical vapor deposition diamond film growth using a kinetic Monte Carlo model and two-dimensional models of microwave plasma and hot filament CVD reactors. *J Appl Phys*. 2010;108:114909. doi: [10.1063/1.3516498](https://doi.org/10.1063/1.3516498)
- [18] Grujicic M, Lai SG. Atomistic simulation of chemical vapor deposition of (111)-oriented diamond film using a kinetic Monte Carlo method. *J. Mater. Sci*. 1999;34(1):7–20. doi: [10.1023/A:1004488818266](https://doi.org/10.1023/A:1004488818266)
- [19] Grujicic M, Lai SG. Multi-length scale modeling of CVD of diamond part I. A combined reactor-scale/atomic-scale analysis. *J Mater Sci*. 2000;35(21):5359–5369. doi: [10.1023/A:1004851029978](https://doi.org/10.1023/A:1004851029978)
- [20] Grujicic M, Lai SG. Multi-length scale modeling of CVD of diamond part II. A combined atomic-scale/grain-scale analysis. *J Mater Sci*. 2000;35(21):5371–5381. doi: [10.1023/A:1004803114048](https://doi.org/10.1023/A:1004803114048)
- [21] Rodgers WJ, May PW, Allan NL, et al. Three-dimensional kinetic Monte Carlo simulations of diamond chemical vapor deposition. *J Chem Phys*. 2015;142(21):214707. doi: [10.1063/1.4921540](https://doi.org/10.1063/1.4921540)
- [22] Semiconductor Technology Research d.o.o. Beograd (STR Belgrade) Belgrade, Republic of Serbia. <https://str-soft.com/>.
- [23] Netto A, Frenklach M. Kinetic Monte Carlo simulations of CVD diamond growth—interlay among growth, etching, and migration. *Diamond Relat Mater*. 2005;14(10):1630–1646. doi: [10.1016/j.diamond.2005.05.009](https://doi.org/10.1016/j.diamond.2005.05.009)
- [24] Valentin A, Brinza O, Farhat S, et al. 3D kinetic Monte-Carlo simulations of diamond growth on (100)

- surfaces. *Diamond Relat. Mater.* 2022;123:108865. doi: [10.1016/j.diamond.2022.108865](https://doi.org/10.1016/j.diamond.2022.108865)
- [25] Williams MDG. Modelling {100} CVD diamond growth using kinetic Monte Carlo [PhD Thesis]. University of Bristol, School of Chemistry; 2022.
- [26] Smith PV, Zheng XM. The clean and hydrogen-terminated (100) and (111) surfaces of diamond and silicon. Vol. 73. In: Howe RF, Lamb RN, Wandelt K, editors. *Surface science*. Springer Proceedings in Physics. Berlin, Heidelberg: Springer; 1993.
- [27] Nepsha VI. Handbook of industrial diamonds and diamond films. Prelas MA, Popovici G, Bigelow LK, editors. New York: Marcel Dekker; 1998. p. 147–192.
- [28] Battaile CC, Srolovitz DJ, Oleinik II, et al. Etching effects during the chemical vapor deposition of (100) diamond. *J Chem Phys.* 1999;111(9):4291–4299. doi: [10.1063/1.479727](https://doi.org/10.1063/1.479727)
- [29] May PW, Mankelevich YA. From ultrananocrystalline diamond to single crystal diamond growth in hot filament and microwave plasma-enhanced CVD reactors: a unified model for growth rates and grain sizes. *J Phys Chem C.* 2008;112(32):12432–12441. doi: [10.1021/jp803735a](https://doi.org/10.1021/jp803735a)
- [30] Mankelevich YA, Ashfold MNR, Ma J. Plasma-chemical processes in microwave plasma-enhanced chemical vapor deposition reactors operating with C/H/Ar gas mixtures. *J Appl Phys.* 2008;104(11):113304. doi: [10.1063/1.3035850](https://doi.org/10.1063/1.3035850)
- [31] Ashfold MNR, Mahoney EJD, Mushtaq S, et al. What [plasma used for growing] diamond can shine like flame? *Chem Commun.* 2017;53(76):10482–10495. doi: [10.1039/C7CC05568D](https://doi.org/10.1039/C7CC05568D)
- [32] Ma J, Richley JC, Ashfold MNR, et al. Probing the plasma chemistry in a microwave reactor used for diamond chemical vapor deposition by cavity ring down spectroscopy. *J Appl Phys.* 2008;104(10):103305. doi: [10.1063/1.3021095](https://doi.org/10.1063/1.3021095)
- [33] Mankelevich YA, Rakhimov AT, Suetin NV. Three-dimensional simulation of a HFCVD reactor. *Diamond Relat Mater.* 1998;7(8):1133–1137. doi: [10.1016/S0925-9635\(98\)00163-0](https://doi.org/10.1016/S0925-9635(98)00163-0)
- [34] Mankelevich YA, May PW. New insights into the mechanism of CVD diamond growth: single crystal diamond in MW PECVD reactors. *Diamond Relat Mater.* 2008;17(7–10):1021–1028. doi: [10.1016/j.diamond.2008.03.022](https://doi.org/10.1016/j.diamond.2008.03.022)
- [35] Guillaume E, Vanpoucke DEP, Rouzbahani R, et al. First-principles investigation of hydrogen-related reactions on (100)–(2×1): H diamond surfaces. *Carbon N Y.* 2024;222:118949. doi: [10.1016/j.carbon.2024.118949](https://doi.org/10.1016/j.carbon.2024.118949)
- [36] Skokov S, Weiner B, Frenklach M. Elementary reaction mechanism for growth of diamond (100) surfaces from methyl radicals. *J Phys Chem.* 1994;98(28):7073–7082. doi: [10.1021/j100079a030](https://doi.org/10.1021/j100079a030)
- [37] Schwaederlé L, Brault P, Rond C, et al. Molecular dynamics calculations of CH<sub>3</sub> sticking coefficient onto diamond surfaces. *Plasma Process Polym.* 2015;12(8):764–770. doi: [10.1002/ppap.201400223](https://doi.org/10.1002/ppap.201400223)
- [38] Garrison BJ, Dawnkaski EJ, Srivastava D, et al. Molecular dynamics simulations of dimer opening on a diamond (2×1) surface. *Science.* 1992;255(5046):835–838. doi: [10.1126/science.255.5046.835](https://doi.org/10.1126/science.255.5046.835)
- [39] Harris SJ, Goodwin DG. Growth on the reconstructed diamond (100) surface. *J Phys Chem.* 1993;97(1):23–28. doi: [10.1021/j100103a007](https://doi.org/10.1021/j100103a007)
- [40] Cheesman A. Investigations into the fundamentals of gas-phase and gas-surface chemistry prevalent in growth of chemical vapour deposited diamond films [PhD Thesis]. University of Bristol, UK.; 2006.
- [41] Frenklach M, Skokov S. Surface migration in diamond growth. *J Phys Chem B.* 1997;101(16):3025–3036. doi: [10.1021/jp9638043](https://doi.org/10.1021/jp9638043)
- [42] Richley JC, Harvey JN, Ashfold MNR. CH<sub>2</sub> group migration between H-terminated 2×1 reconstructed {100} and {111} surfaces of diamond. *J Phys Chem C.* 2012;116(14):7810–7816. doi: [10.1021/jp300454r](https://doi.org/10.1021/jp300454r)
- [43] Oleinik II, Pettifor DG, Sutton AP, et al. Theoretical study of chemical reaction on CVD diamond surfaces. *Diamond Relat Mater.* 2000;9(3–6):241–245. doi: [10.1016/S0925-9635\(99\)00312-X](https://doi.org/10.1016/S0925-9635(99)00312-X)
- [44] Stukowski A. Visualization and analysis of atomistic simulation data with OVITO – the open visualization tool. *Modelling Simul Mater Sci Eng.* 2010;18(1):015012. doi: [10.1088/0965-0393/18/1/015012](https://doi.org/10.1088/0965-0393/18/1/015012)